

An improvement to Global Tractography Using Anatomical Priors

Didrik Skiöldebrand

Master's thesis
2014:E6

Faculty of Engineering
Centre for Mathematical Sciences
Mathematical Statistics

Abstract

Tractography is a visualization technique which reconstructs and models neural fibers in the white matter of the brain based on data from diffusion magnetic resonance imaging. It is already used locally to model parts of dominant fiber pathways but global methods are also emerging which aim to reconstruct all the brain fibers simultaneously.

In this thesis we have attempted to improve the current state of the art of Global Tractography by introducing three principles:

- Anatomical Priors
- Introduction of fiber weights
- Reduced complexity

Our approach uses an optimization method based on Markov Chain Monte Carlo (MCMC) and Simulated annealing in order to fit a set of plausible initial fiber trajectories to a dataset acquired by diffusion MRI. Our method was compared to the state of the art global tractography method known as the Gibbs Tracker in a phantom study using conventional global tractography evaluation methods. In a second test, we also try the method on an in-vivo dataset of a human brain and derive the connectivity matrix with corresponding network parameters. Our approach showed considerable improvements in decreasing the amount of wrong fibers and reduced computational time. However the method still struggles to eliminate certain false but plausible connections. To remedy this, several improvements to the MCMC sampler are suggested for future work.

Keywords: Diffusion MRI, fiber tracking, global tractography, Markov Chain Monte Carlo, simulated annealing

Acknowledgements

First I would like to thank Professor Jean-Philippe Thiran for granting me the opportunity to come to EPFL in the first place. Without you this thesis would not be possible. Secondly and just as important I would like to thank Alessandro Daducci and Alia Lemkaddem for invaluable support and endless patience with me. Thank you for the warm welcome and always granting me the time to come by your office. Thank you all at Signal Processing Laboratory 5 for the great working environment and friendships. Finally, I would like to thank professor Andreas Jakobsson for taking on and approving my project as an examiner.

Abbreviations

CC - Corpus Callosum

DPPRA - Douglas Peucker Point Reduction Algorithm

DTI - Diffusion Tensor Imaging

DWI - Diffusion Weighted Imaging

EPFL - École Polytechnique Fédérale de Lausanne

HARDI - High Angular Resolution Diffusion Imaging

MCMC - Markov Chain Monte Carlo

MRI - Magnetic Resonance Imaging

ODF - Orientation distribution function

ROI - Region of interest

SA - Simulated Annealing

Contents

1	Introduction	1
1.1	Background	1
1.2	Objectives	1
1.3	Outline of Thesis	2
2	State of the Art	3
2.1	Basics of Magnetic Resonance Imaging	3
2.2	Diffusion MRI	5
2.3	Diffusion MRI Local Reconstruction	6
2.3.1	Diffusion Weighted Imaging	6
2.3.2	Diffusion Tensor Imaging	7
2.3.3	High Angular Resolution Diffusion Imaging (HARDI)	8
2.4	Tractography	10
2.4.1	Local Tractography	10
2.4.2	Global Tractography	12
2.5	Brain Connectivity Analysis	13
3	The Proposed Model	15
3.1	Markov Chain Monte Carlo Optimization	19
3.1.1	Markov Chain Monte Carlo	19
3.1.2	Simulated Annealing	19
3.1.3	The Metropolis Hastings Algorithm	20
3.2	Model Parameter Selection	21
3.2.1	Proposal Parameters	21
3.2.2	Spline and Gaussian Smoothing Parameters	22
3.3	Implementation	23
3.4	Datasets and Evaluation	23
3.4.1	FiberCup	24
3.4.2	Tractometer	24
3.4.3	In-vivo Brain Data	25
4	Results and Discussion	26
4.1	FiberCup Dataset	26
4.2	In-vivo Data	33
5	Conclusions	35

1 Introduction

1.1 Background

Tractography is a 3D modeling technique used to visually represent the neural pathways in the white matter of the brain using data collected by diffusion magnetic resonance imaging (dMRI). The white matter of the brain consists primarily of bundles of myelinated nerve cells which have a fibrillar structure much like skeletal muscle cells. Diffusion MRI measures the motion of hydrogen atoms within water molecules which diffuse only along the direction of these fibers, revealing these pathways. Tractography has been given increased interest due to its usefulness in clinical applications which include [4]:

- Stroke
- Multiple sclerosis (MS)
- Neurodegenerative diseases
- Neurosurgical applications
- Spinal cord disorders

Tractography can also be used on a global scale (referred to as global tractography) to create a connectivity map between distinct regions of the brains gray matter called a *connectome*, a term referring to a comprehensive map of neural connections in the brain [15]. The connectome can be used to study the brains structural connectivity using conventional mathematical graph theory by extracting network parameters much like studying traffic, computer or social networks [30].

Global tractography and connectome analysis is a rapidly developing field still in its infancy with much waiting to be explored.

1.2 Objectives

The objective of this thesis was an attempt to develop a probabilistic global tractography reconstruction method based on the current state of the art; which not only performs better than the current state of the art, but also is a starting point for a novel way to study the connectome: namely to analyze a set of possible connectomes by exploring around an optimal solution using Markov Chain Monte Carlo sampling, thus obtaining a distribution of possible connectomes. This new approach by allowing a degree of uncertainty to the end solution, is potentially very useful as currently there exists no absolute ground truth of the connections in real brain tissues.

This thesis was written at the Signal Processing Laboratory 5 (LTS5) at École Polytechnique Fédérale de Lausanne (EPFL) in Lausanne Switzerland which conducts research in structural brain connectivity analysis using tractography where new global reconstruction algorithms are being developed.

1.3 Outline of Thesis

Chapter 2 introduces the reader to the topic of MRI and more specifically diffusion MRI. First the basic physics behind MRI is explained along with the different imaging and acquisition techniques used for diffusion MRI. The chapter then continues by providing a thorough background for tractography.

Chapter 3 presents the proposed method itself, along with the calibration of parameters and datasets used for evaluation of the model.

Chapter 4 presents and discusses the results of the developed method. Here we elaborate over the method's advantages and limitations and also outlines for future work are discussed.

Chapter 5 is a concluding discussion over the results where also improvements and future work are suggested.

2 State of the Art

2.1 Basics of Magnetic Resonance Imaging

The following section is a brief overview of the physics which enable magnetic resonance imaging and is mainly a summary of the theory presented in [19]. Magnetic resonance imaging (MRI) is an imaging technique used to create image volumes in which slices can be viewed at any location or direction. The fundamental property which enables MRI is spin. One can think of spin as a particle rotating around its own axis causing it to behave like a tiny magnet with a north and a south pole. This generates a magnetic moment vector \mathbf{m} that is parallel to the rotation axis.

The direction of this magnetic moment \mathbf{m} is usually considered random because

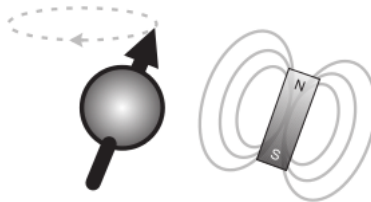


Figure 1: Nuclear spin causing the particle to behave like a tiny magnet [19]

the orientation of the individual particles is unknown, so the total magnetic moment over several particles is zero.

When a group of particles are placed under an external magnetic field \mathbf{B} , the direction of the spin vectors will align themselves either parallel or anti-parallel to the outer field, giving rise to two energy states: a low energy state consisting of parallel spins and a high energy state consisting of anti-parallel spins.

As a consequence of the laws of thermodynamics, in which nature strives to

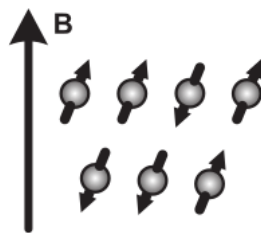


Figure 2: Spins aligned parallel or anti-parallel with the external magnetic field [19].

minimize its energy, the number of spins in the lower energy state will slightly outnumber the ones in the higher energy state. The ratio between the number of particles in each state are given by the Boltzmann distribution

$$\frac{N^-}{N^+} = e^{\frac{-E}{kT}}, \quad (1)$$

where N^- represents the number of spins in the higher energy level, N^+ the number of spins in the lower energy level, k is Boltzmann's constant and T is the temperature in Kelvin.

Once all the particles are aligned and placed in these two distinct states, it is possible for the particles in the lower state to transition to the higher state by absorbing photons containing the exact amount of energy as the energy gap between the states.

On a macroscopic scale, the slight overweight of particles in the lower energy state will result in a net magnetization vector \mathbf{M} pointing in the direction of the external magnetic field \mathbf{B} . When acquiring an MRI image, a radio frequency

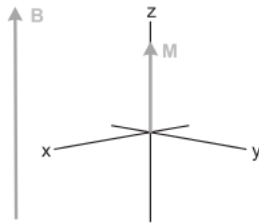


Figure 3: Net macroscopic magnetization vector \mathbf{M} pointing in the direction of the main magnetic field \mathbf{B} [19].

pulse (RF) is applied towards the area that is to be examined. This pulse is much weaker than \mathbf{B} and is applied through a rotating reference frame perpendicular to \mathbf{B} . This RF-pulse causes individual particles in the area to absorb the quanta of energy required to transition from the lower energy state to the higher state by changing their alignment to \mathbf{B} , thus causing \mathbf{M} to spiral away from its initial alignment with \mathbf{B} and end up rotating around \mathbf{B} at a distance proportional to the time length of the RF-pulse. After a certain length of time, \mathbf{M} will have rotated 90 degrees and will be perpendicular to \mathbf{B} . The net magnetization \mathbf{M} also starts to dephase since different particles will experience a slightly different magnetic field. This is usually referred to as phase coherence. When the RF-pulse is

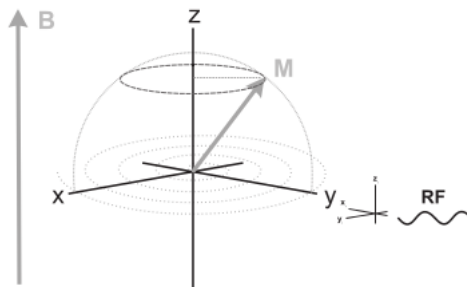


Figure 4: RF pulse applied through a rotating reference frame causing the net macroscopic magnetization to spiral away from the \mathbf{B} [19].

removed, particles will begin to return to their lower energy state, causing \mathbf{M} to gradually return to its initial position aligned with \mathbf{B} . This loss of energy is

then detected by a coil in the MRI-scanner which is the information used to produce an image. The information gathered by the scanner is:

- The energy release
- The time passed until \mathbf{M} returns to its "normal" alignment, called the T1 relaxation.
- The time passed until the phase coherence is lost, called T2 relaxation time.

In clinical MRI, the RF-pulse is chosen to coincide with the frequency corresponding to energy difference required for hydrogen protons in water molecules to transition between energy states. The energy release is then an estimate of the number of hydrogen nuclei, which in principle corresponds to the amount of water in the examined volume. The T1 relaxation gives information on the chemical surrounding of the water and the T2 relaxation reflects the surroundings of each individual atom, which gives a different contrast. With these variables it is possible to separate tissues since they will show different characteristics in T1 and T2 relaxation time. Images acquired using the different relaxation are usually called, respectively, T1 weighted and T2 weighted.

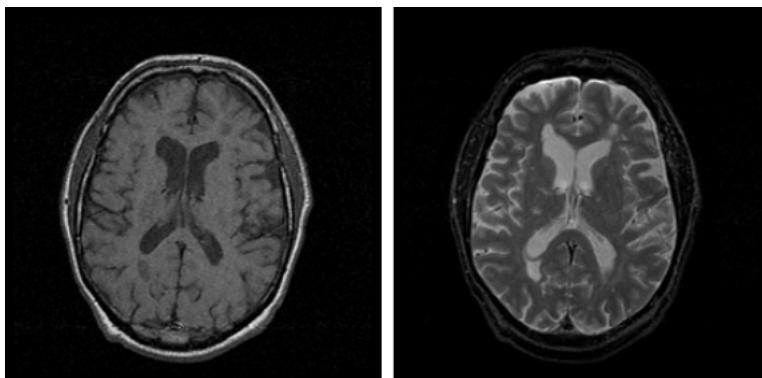


Figure 5: Left: T1 weighted axial slice. Right: T2 weighted axial slice [19].

2.2 Diffusion MRI

Diffusion MRI is an extension of conventional MRI focused on mapping the diffusion process of molecules as a cause of Brownian motion. Brownian motion, which was discovered by Einstein in 1903 [11], refers to the random motion of molecules resulting from thermal energy. In a glass of water, the motion of the water molecules are completely random and is limited only by the boundaries of the container. This motion is best described by a displacement distribution describing the proportion of molecules that undergo displacement in a specific direction. Diffusion of a molecule in a homogeneous medium is well described in having a Gaussian distribution. In neuronal tissue however, with its fibrillar structure, the movement of the molecules are hindered to a greater extent in the direction perpendicular to the axonal orientation than parallel to it, thus

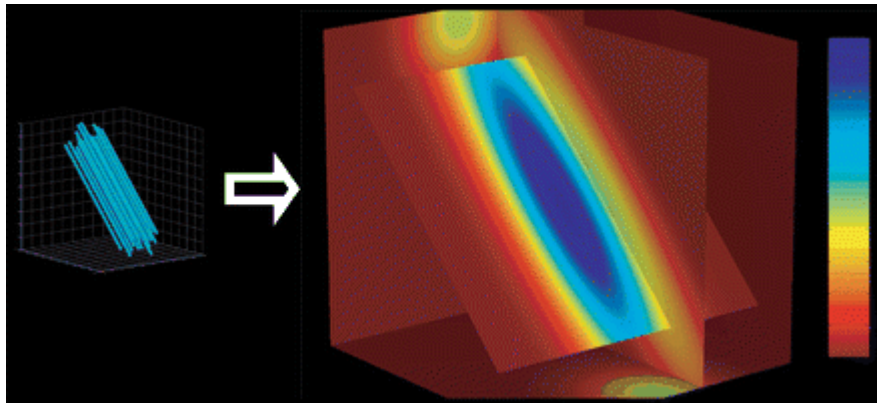


Figure 6: A typical diagram showing the diffusion probability within a voxel with axons aligned in the same direction. Note that the probability is color coded due to the fact that the three spatial dimensions are used for representing the positions of the diffusion [16].

resulting in an according distribution in which the pathway of the fiber is revealed. Diffusion MRI is able to depict this motion by adding a sequence to the normal MRI procedure that involves applying a gradually increasing gradient field in the same direction as the RF-pulse introducing an additional phase shift to the magnetic moment proportional to the molecular displacement along that gradient direction [16]. The more a molecule has moved in the gradients direction during the acquisition, the larger the phase shift will be. This leads to a loss of signal which is used to measure the diffusion.

2.3 Diffusion MRI Local Reconstruction

In diffusion MRI, the objective is to obtain the 3D orientation distribution function (ODF) of the water diffusion for each 3D voxel coordinate of the volume studied. An ODF may be considered as a deformed sphere whose radius in a given direction is proportional to the sum of values of the diffusion PDF in that direction [16]. To further ease visualization, the surface of the ODF is color coded according to a diffusion direction. Most commonly used is $[x, y, z] = [\text{red}, \text{green}, \text{blue}]$.

Now follows a brief overview of diffusion MRI techniques from the simplest to the most sophisticated technique [16]. This is important to understand as it is this information which is used to later reconstruct the fiber tracks in tractography.

2.3.1 Diffusion Weighted Imaging

Diffusion weighted imaging (DWI) is the basic component needed for any of the more sophisticated imaging techniques. It is simply the unprocessed result of an acquisition using a single gradient field in one specific direction. Figure 8 shows a typical diffusion weighted image where darker regions represent areas with high diffusion along the specific acquisition gradient direction and lighter parts represent less diffusion. Even though this is not as informative as having

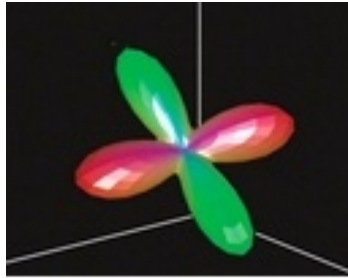


Figure 7: A typical orientation distribution function (ODF) representation in a single voxel [2]

an image with the ODF of the diffusion in every voxel, DWI is still applied clinically for stroke investigations which cause damage to neural pathways and restrictions in water movement.

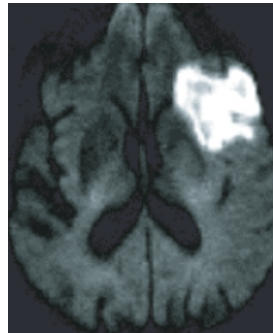


Figure 8: A typical diffusion weighted image. The darker regions show increased diffusion in the specific acquisition direction while the lighter regions show reduced diffusion. This specific image shows a brain with acute ischaemia. The diffusion image clearly shows decreased diffusion in the infarcted tissue. [3].

2.3.2 Diffusion Tensor Imaging

Normally more information than the DWI is required when studying the structural connectivity of the brain. Diffusion tensor imaging (DTI) is the most standard way to view this [2].

Assuming plain diffusion MRI, the diffusion effect on the MRI signal is a scalar value A which depends on the diffusion D and the "b-factor" which characterizes the gradient pulses (timing, amplitude and shape) used in the MRI sequence. Since the diffusion is assumed to be a 3D-Gaussian process it is modeled as a tensor.

$$A = \exp(-bD). \quad (2)$$

Where D is the diffusion tensor which describes the diffusion along each direction.

$$D = \begin{bmatrix} D_{xx} & D_{xy} & D_{xz} \\ D_{yx} & D_{yy} & D_{yz} \\ D_{zx} & D_{zy} & D_{zz} \end{bmatrix} \quad (3)$$

This tensor is symmetric ($D_{ij} = D_{ji}$) where $i, j = x, y, z$ and from it several useful measurements can be extracted. The mean diffusion is derived from the trace (which is the sum of the diagonal) of the tensor while the principle direction of the diffusion maximum can be obtained by computing the eigenvectors and eigenvalues of the tensor [2]. Eigenvectors which are orthogonal to one another will, together with the eigenvalues which are ordered as $\lambda_1 \geq \lambda_2 \geq \lambda_3$ describe the properties of the tensor, resulting in a diagram much like figure 9.

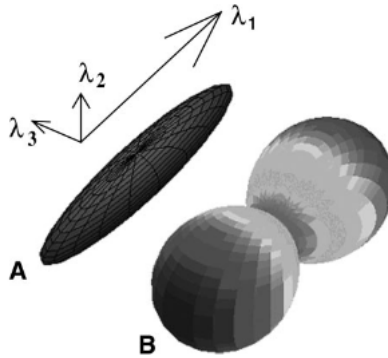


Figure 9: Diagram of diffusion of tensors. In *A*, the diffusion tensor is shown as an ellipsoid with its principle axis along the eigenvectors ($\lambda_1, \lambda_2, \lambda_3$) characterizing the strength of diffusion in each direction. In *B* the diffusion tensor is shown as an ODF [16]

The relationship between the eigenvalues reflect the characteristics of diffusion. The shape is represented by a scalar value known as *fractional anisotropy* which is computed by comparing each eigenvalue to the mean of all of the eigenvalues $\langle \lambda \rangle$ [2].

$$FA = \sqrt{\frac{3}{2}} \sqrt{\frac{(\lambda_1 - \langle \lambda \rangle)^2 + (\lambda_2 - \langle \lambda \rangle)^2 + (\lambda_3 - \langle \lambda \rangle)^2}{\lambda_1^2 + \lambda_2^2 + \lambda_3^2}}, \quad (4)$$

where FA is the fractional anisotropy.

The DTI model performs well in regions where there is only one fibre population (i.e. fibres are aligned along a single axis), where it gives a good depiction of the fibre orientation. However, it fails in regions with several fibre populations aligned along intersecting axes, such as fiber crossings, because it cannot be used to map several diffusion maxima at the same time. Figure 11 shows a sketch of a DTI reconstruction of a fiber crossing; note that since there are diffusion maxima, the tensor is modeled as a sphere.

2.3.3 High Angular Resolution Diffusion Imaging (HARDI)

In order to overcome the problems of complicated fiber scenarios, imaging techniques that provide higher angular resolution are needed. High angular resolution diffusion imaging (HARDI) is a collection name of these techniques which obtain more diffusion information by an increased number of acquisitions, with

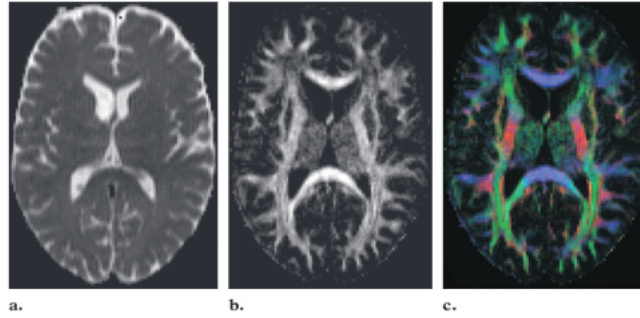


Figure 10: Extraction of scalar values from DTI. (a) shows the mean diffusion calculated by the trace of the tensor. (b) shows the fractional anisotropy, which is computed from the eigenvalues and eigenvectors of the tensor. (c) Color coded fractional anisotropy better representing diffusion along the x -, y -, z and z -axis [16].

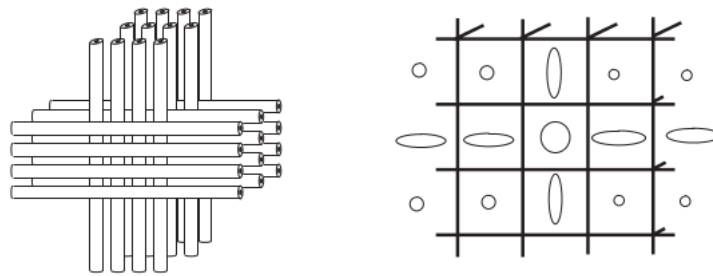


Figure 11: Left:A fiber crossing. Right: Sketch of DTI reconstruction of fiber crossing. The round tensor in the middle shows how the tensor is unable to represent the two fiber directions simultaneously [19].

gradients that vary in strength and direction. The cost of this is an increased acquisition time around 10 times longer than DTI. For global tractography this imaging technique is much more preferred regardless of the longer acquisition time. With this increased amount of information it is possible to extend the single tensor of DTI (2) to a *multitensor* model consisting of a several tensors modeling the diffusion in individual compartments [28].

$$A = \sum_j f_j \exp(-bD_j), \quad (5)$$

where f_j is the apparent volume fraction of the voxel with diffusion tensor D_j . Each tensor which has an orientation to fit a major diffusion direction will then contribute to modeling diffusion proportional to its corresponding volume fraction.

2.4 Tractography

While the imaging techniques explained in the previous chapter focuses on acquiring the diffusion tensor or ODF in each voxel, tractography is the next step of post processing in which this information is used to construct and visualize neural tracts (bundles of fibers) traversing through each voxel. Tractography is currently the only noninvasive in-vivo method available for studying the fiber tract anatomy of the human brain [19]. Tractography techniques can be divided into two subgroups: local and global tractography.

2.4.1 Local Tractography

Local methods reconstruct fibers one by one independently, without taking into consideration the influence of neighboring fibers. Because of this, local tractography is mostly used to study white matter in specific predetermined regions where specific tracts are of interest, which is useful for numerous medical applications explained in the introduction. There are several different approaches for local tractography which fall into two subcategories [22].

Line Propagation Methods

The first category, *Line propagation methods*, are deterministic methods based on line propagation algorithms using the local tensor information from each voxel obtained from DTI. The fiber pathways are reconstructed by propagating through each voxel from a designated starting point with the assumption that the fiber continues in the maximum diffusion direction provided by the diffusion tensor. Tractography algorithms use this information to track the whole white matter pathway by inferring the continuity of fiber paths from voxel to voxel [2]. The pathway is reconstructed progressively until certain stopping criteria are met. Mainly two stopping criteria are used: the first one is called the *angular threshold*. If the angle between two diffusion directions in adjacent voxels is larger than a certain threshold, the propagation is terminated. This is used to prevent implausible pathways such as a fiber that turns too sharply. The second stopping threshold, the *anisotropy threshold*, stops the propagation when it reaches a voxel with very low to no anisotropy. Low anisotropy areas are either

along the propagation route resulting from local noise in each voxel [22].

Local reconstruction methods are therefore unsuitable in their current state

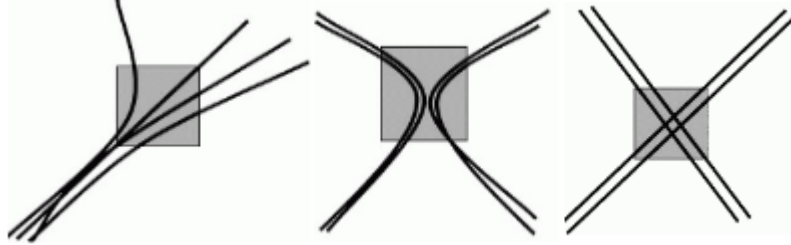


Figure 13: The figure shows the three problematic scenarios for local tractography methods. Left: Branching scenario of fibers. Middle: Kissing scenario of fibers. Right: Crossing of fibers [1].

for global tractography. This brings us to the second subgroup of tractography algorithms, namely global methods.

2.4.2 Global Tractography

Global tractography, which is the category which the developed model for this thesis falls within, represents a new approach to identifying brain networks. It involves the simultaneous reconstruction of all the fibers which align with the directions of least hindrance to water diffusion in the brain by finding a solution that best fits the measured diffusion data. This is achieved by minimizing a global cost function which is represented by the L_2 -norm of the difference between the reconstructed model of fibers and the measured data consisting of ODFs in each voxel. The global approach has a better ability to resolve local fiber orientations, as it considers more than just the local information. Because of this, global tracking may be more stable than local methods in the presence of noise and imaging artifacts in the data [20]. Among existing global tractography methods, there are especially two which are noteworthy of mentioning.

The Gibbs Tracker

The Gibbs tracker [27][18] is a probabilistic reconstruction method with origins in statistical physics, hence the name. The reconstructed fibers are built with small line segments that introduce the diffusion anisotropy which are randomly inserted into the image. These elemental segments bind together during the optimization forming fibers. Their orientation and number are adjusted simultaneously to match the data. This behavior is governed by an interaction between line segments and by an increasing match to the measured data.

The Spin-Glass Model

The idea behind the spin glass model framework [13] is to parameterize a set of white matter fibers by small segments called spins. These spins are allowed to move, rotate and duplicate. They are controlled by three potential energies: a diffusion, an interaction and a generative potential. The diffusion potential

attracts spins towards the main fiber directions, while the interaction potential encourages them to form longer chains of minimal curvature. The generative potential prevents a spin chain to end inside the domain by allowing the creation of new spins. The optimal spin configuration is finally retrieved by a global minimization procedure.

Global tractography is a new emerging approach to tractography. Although promising, global tractography currently has obstacles to overcome and needs to be rigorously validated in order to prove to be clinically feasible. The main problem with global methods is that they have a very high computational cost due to the large size of the solution space. The issue of validation is also important because currently there exists no absolute ground truth on the connections existing in real brain tissues. Even if the reconstruction algorithms prove to work well on a phantom, it is not guaranteed to perform as well on real brain data with its many more complicated fiber scenarios.

In contrast to local methods, global methods are intended to be used when studying the structural connectivity of the brain between different regions. The neural pathways modeled by tractography which connect distinct gray matter areas can be used to create a comprehensive map of the brains neural connections called a *connectome*.

2.5 Brain Connectivity Analysis

This section will give an overview of how the structural connectivity of the brain is studied using network parameters given a connectome. Over the past decade, the study of networks has rapidly expanded across a number of scientific disciplines, including neuroscience, due to the realization that the brain as a complex interconnected and dynamic system can be analyzed using mathematical and statistical tools developed in graph theory.

Graphs are mathematical descriptions of a system composed by interconnected elements, comprising of nodes and edges. See figure 14 for a visual representation of a graph. The nodes are the fundamental functional units of the system, edges are the connections links between each node. In our case with the brain, nodes are the regions of the brains gray matter which are to be connected and edges are the fiber pathways modeled by tractography. It is the characteristics of the edges which define the network properties. The complete set of nodes and edges are represented in a connection matrix [30]. These connection matrices can be either *unweighted* or *weighted*. The unweighted (also known as binary) connection matrix's elements are either 0 or 1 determining if there exists a connection between the nodes or not. The value of the weighted matrix's elements are determined by how strong of a connection exists between two nodes.

There are many measures which can be calculated for a network but in this thesis we will only focus on the core measures [12].

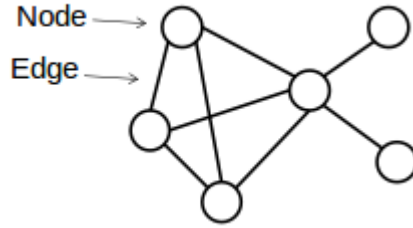


Figure 14: Graphical representation of a network (or graph) [12]

Strength (k)

The *strength* of the node corresponds to the number of edges which connect to it, which is also the number of nodes which directly connect to it.

Clustering Coefficient (C)

This is the main measure of local structure of a network which can be calculated for individual nodes or the entire network. The clustering coefficient c_i of node i with strength k_i can be defined as the ratio of the actual number of edges between neighbors of i , which is defined as e_i , and the maximum number of possible number of edges between those edges.

$$c_i = \frac{2e_i}{k_i(k_i - 1)} \quad (7)$$

The clustering coefficient C of the network is the average of all individual clustering coefficients. The clustering coefficient varies between 0 and 1. A high C means that neighboring nodes are well connected which means that the loss of an individual node will have little impact on the structure of the network.

Characteristic Path Length (L)

The characteristic path length of a network is the average distance between all pairs of nodes

$$L = \frac{1}{N(N-1)} \sum_{i,j \in N, i \neq j} d_{i,j} \quad (8)$$

where N is the total number of nodes and $d_{i,j}$ is the path length between two nodes i and j which is defined by the smallest number of edges connecting them. This is a measure indicating how well integrated a network is and how easy information can flow within the network.

Based on these core network measures, it is possible to distinguish the network type, identify different hubs or compare them to healthy or pathological networks.

3 The Proposed Model

Denote the set of all fibers in our model by \mathcal{M} and the measurement data by $D(x, \mathbf{n}) = S(x, \mathbf{n})/S_0(x, \mathbf{n})$ where $S(x, \mathbf{n})/S_0(x, \mathbf{n})$ is a diffusion weighted HARDI signal at position x with gradient direction \mathbf{n} normalized by the measurement without diffusion weighting. The objective is to explore the different states of the model to find the combination of fibers which best fits the data. Concretely this is a combinatorial optimization problem. The optimal solution is found by exploring the distribution of possible solutions and sampling candidates from the posterior probability $P(\mathcal{M}|D)$ with respect to \mathcal{M} . According to Bayes theorem the posterior distribution is given by

$$P(\mathcal{M}|D) \propto P(D|\mathcal{M})P(\mathcal{M}). \quad (9)$$

Where $P(\mathcal{M})$ is the prior and $P(D|\mathcal{M})$ is the data likelihood.

The prior information $P(\mathcal{M})$ used in the model was mainly two things:

- The fibers start and end up in the gray matter of the brain.
- The fibers will strive to be as smooth as possible and will choose the most energy minimizing path in respect to the diffusion between two regions of interest.

The developed method incorporates this by generating plausible initial trajectories using an initialization method based on Dijkstra’s shortest path algorithm [9]. The algorithm works in such a way that it for each considered voxel, evaluates the pathways between evenly distributed nodes on the voxel edges, and returns the ones which have the least cost in respect to following the diffusion direction given by the ODF and the pathways curvature.

The data likelihood $P(D|\mathcal{M})$ was derived from the Gibbs distribution of statistical physics which is used to determine the probability of a certain state given the value of the energy in the system [18].

$$P(\mathcal{M}|D) = e^{-E(\mathcal{M},D)/T}. \quad (10)$$

Here the energy E expresses the similarity between the model in its current state and the measured data. Consider a single fiber in the model \mathcal{M} evaluated as segments of length l evenly along it. Each segment contributes additively in reconstructing the ODF in neighboring voxels with an intensity proportionate to a Gaussian distribution centered in that voxel.

$$\rho_{seg}(\mathbf{x}, \mathbf{n}) = e^{-bD} e^{-|\mathbf{x}-\mathbf{x}_i|^2/\sigma^2} \quad (11)$$

The first exponential is the expression of the ODF according to the diffusion multitensor model explained in 2.3.3 and the second exponential is the Gaussian distribution centered in \mathbf{x} of that voxel, where \mathbf{n}_i and \mathbf{x}_i are the orientation and position of the center the segment. The procedure of multiplying by a Gaussian distribution is referred to as Gaussian smoothing and figure 15 attempts to visualize the principle.

For one fiber, consisting of individual segments, its contribution to the total

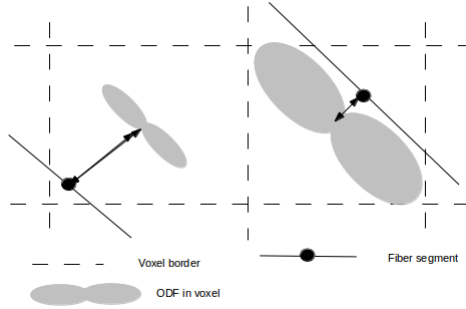


Figure 15: Simple figure showing logic behind Gaussian smoothing. The closer the segment is to the center of the voxel, the larger it contributes to the calculated ODF

signal is simply the sum of all of its segment's contributions multiplied by a weight $w \geq 0$

$$\rho_{\mathcal{M}}(x, \mathbf{n}) = w \sum_{seg} \rho_{seg}(x, \mathbf{n}). \quad (12)$$

The weight parameter is not initially known and is one of the parameters which is to be set and optimized by the method according to how well that fiber fits the signal. One can consider the weight as a measure of the signals amplitude or how strong connection that specific fiber has. If we have a voxel with several fibers passing through it, the algorithm is supposed to apply a high weight to the fibers fitting the data well and a low weight to ones not fitting. Also, two correctly overlapping fibers can instead merge as one if we merge their weights and remove the other fiber. This will prune away unnecessary and incorrect fibers when fitting them to the measured data.

An obvious advantage of using weights is that we can use less fibers to represent connections instead of letting the strength of a connection be determined by the amount of fibers between regions.

The energy in the likelihood distribution expression (10) is the L_2 -norm of difference between the reconstructed signal and the data.

$$E(\mathcal{M}, D) = \|\rho_{\mathcal{M}} - D\|_{L_2}^2. \quad (13)$$

This equation will in the future be referred to as the *cost function*.

In order to minimize the number of parameters describing the fibers, a spline formulation was used to represent them; more specifically, the Catmull-Rom (CR) spline formulation with five control points [6]. This has previously proved to be successful in other tractography models [17] but then only for reconstructing certain connections. This model is the first attempt to use splines to model fibers in the scale of the entire connectome.

For the uninitiated user, a spline is a mathematical way of representing a curve, by specifying a series of points at intervals along the curve and defining a function that allows additional points within an interval to be calculated.

CR splines are a family of cubic interpolating splines formulated such that the tangent at each control point P_i is calculated using the previous and next control point on the spline, $\tau(p_{i+1} - p_{i-1})$. The full representation is given by

$$\mathbf{P}(s) = [1 \ u \ u^2 \ u^3] \begin{bmatrix} 0 & 1 & 0 & 0 \\ -\tau & 0 & \tau & 0 \\ 2\tau & \tau - 3 & 3 - 2\tau & -\tau \\ -\tau & 2 - \tau & \tau - 2 & \tau \end{bmatrix} \begin{bmatrix} \mathbf{p}_{i-2} \\ \mathbf{p}_{i-1} \\ \mathbf{p}_i \\ \mathbf{p}_{i+1} \end{bmatrix}$$

CR splines are widely used in graphical applications thanks to three useful properties. First, the curve will always interpolate through its control points which gives good control of the spline when placing or moving its control points. Second, each control point only effects a small neighborhood around itself. This means that one only has to re-parameterize the affected section of the spline instead of its entirety granting computational speed.

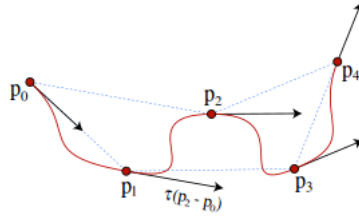


Figure 16: A typical Catmull-Rom spline [6]

The Douglas-Peucker point reduction algorithm [10] (DPPA) was used to simplify the control points of each fiber to the number of points needed for the spline formulation (five in our case). Here follows a description of the algorithm along with figure 17 to help visualize the procedure.

Initially the algorithm is given a fiber. It then automatically marks the first and last point to be kept. It then finds the point that is furthest from the line segment with the first and last points as end points, (distance b in figure 17). If that point is closer than a set threshold value ϵ to the line segment it can be discarded without the simplified curve being worse than ϵ .

If the point is greater than ϵ from the approximation line, then that point must be kept. The algorithm then recursively calls itself with a new fiber where the first point and evaluated point act as the new first and last point. When the recursion is completed a new output curve can be generated consisting of all the points that have been marked as kept.

Since it was not possible to predefine the amount of points to reduce to, the DP-algorithm had to run several times on the same fiber and increase epsilon each time. If the fiber was reduced by too many points it was disregarded and not included in the initial setup. This was deemed as an acceptable loss due to the large number of fibers included in the shortest path initialization.

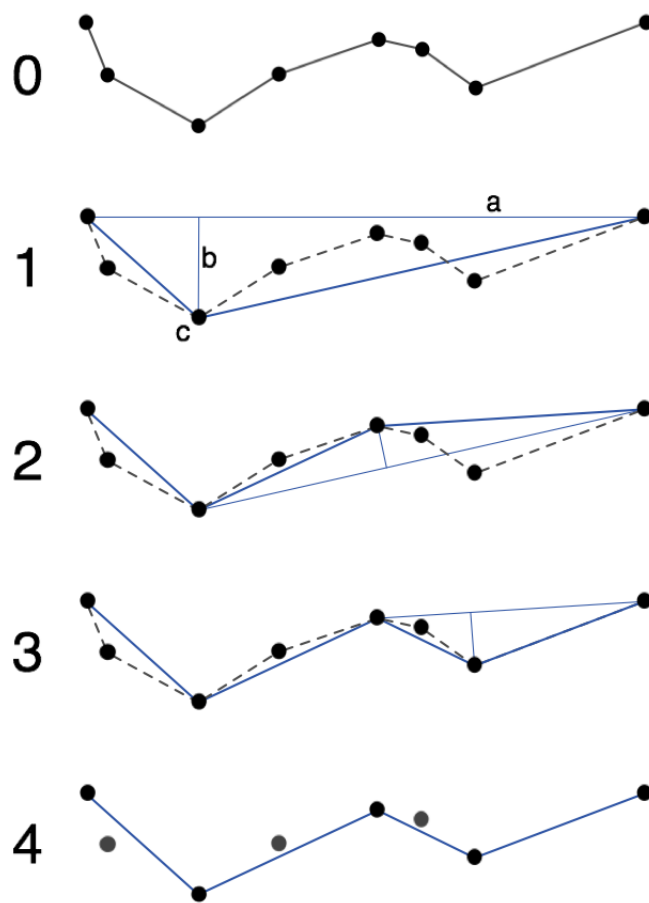


Figure 17: The different steps of the Douglas-Peucker point reduction algorithm [10]

3.1 Markov Chain Monte Carlo Optimization

The optimization procedure used for the method was Markov Chain Monte Carlo (MCMC) combined with simulated annealing.

3.1.1 Markov Chain Monte Carlo

Markov Chain Monte Carlo is the most used method for simulating from a complicated and/or high-dimensional distribution. The basic idea is to construct a Markov Chain that has f as a stationary distribution, where f is the distribution we want to simulate from [29].

3.1.2 Simulated Annealing

Simulated annealing is an expansion of Markov Chain Monte Carlo (MCMC) used when the Markov chain's movement through the state space is hindered by regions of low probability, thus preventing it to converge to their equilibrium distribution within a reasonable time.

The method was introduced for optimization problems when the goal was to sample from the Boltzmann distribution $P(E) = \exp^{-E/kt}/Z$ for a system at temperature zero, in which the probability is concentrated at the states of minimal energy [24].

The term "Simulated Annealing" is inspired from metallurgy in which slow cooling (annealing) is used when forging metal in contrast to fast cooling (quenching) to minimize defects. When a Markov chain simulation is used to sample from the Boltzmann distribution given some energy function, as in our case 13, the analogous procedure is to gradually reduce the temperature from an initial high one to a temperature value at which we wish to sample. The initial high temperature will allow the Markov chain to wander more freely and hopefully overcome energy barriers.

For our model this involves sampling new candidates from the posterior distribution (9) and accepting them if they better fit the data while successively lowering the temperature term T in (10). As T becomes lower, it is more likely to sample from the maximum of the posterior distribution.

The success of simulated annealing lies in large part on the choice of a suitable cooling schedule and initial temperature. Common cooling schedules include:

- Logarithmic cooling: $T_{i+1} = T_0/\log(i)$
- Geometric cooling: $T_{i+1} = \alpha T_i$, $0 < \alpha < 1$
- Exponential cooling: $T_{i+1} = T_0 e^{-\alpha i}$, $\alpha > 0$.

There is no exact method in determining which schedule is "correct" for each application, and it is mostly fine tuning or trial and error which determines the most suitable one [24]. An important common trait is that the temperature should always be decreasing for each iteration. For the developed model, an exponential cooling schedule was used since it had been proven successful for

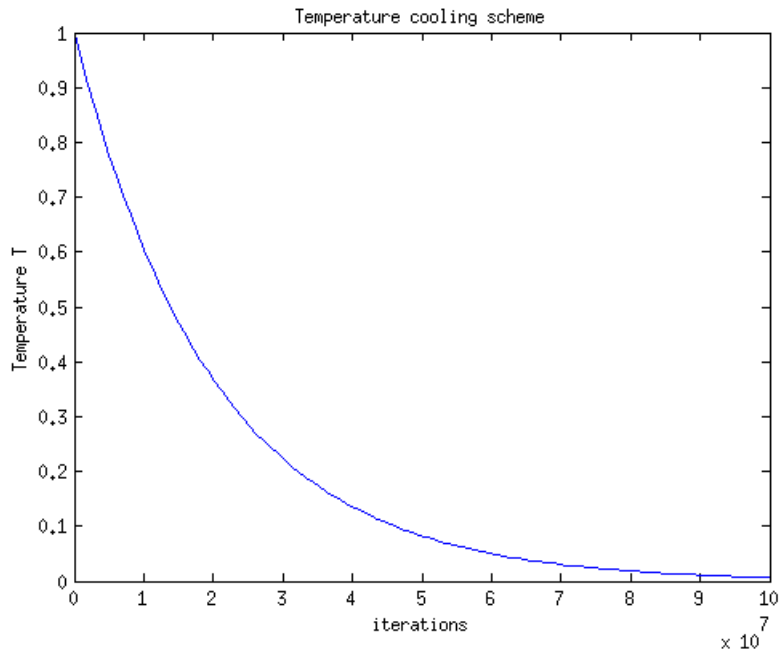


Figure 18: Temperature cooling scheme for simulated annealing

the Gibbs tracker [27]. The starting temperature T_0 was set to 1 $T_0 = 1$ and the cooling parameter was set so that the stop temperature was $T_{stop} = 10^{-3}$.

3.1.3 The Metropolis Hastings Algorithm

Sampling from the posterior distribution was done using the Metropolis Hastings (MH) sampler which is an established technique when dealing with high dimensional distributions [29]. It works as follows: starting from a current state of the model \mathcal{M} , modify the model and transfer it to a new state \mathcal{M}' according to a proposal distribution q . Then calculate the ratio given by

$$\alpha = \frac{P(\mathcal{M}'|D)q(\mathcal{M}|\mathcal{M}')}{P(\mathcal{M}|D)q(\mathcal{M}'|\mathcal{M})}. \quad (14)$$

If $\alpha > 1$ the new state is accepted, otherwise it is accepted with the probability α . The expression α balances the Markov chain to both sample more probable states while at the same time exploring states which are harder to reach. The first half of the expression

$$\frac{P(\mathcal{M}'|D)}{P(\mathcal{M}|D)}$$

will give a higher α if the proposed state \mathcal{M}' is more probable than \mathcal{M} , i.e., $P(\mathcal{M}'|D) > P(\mathcal{M}|D)$. The second half of the expression

$$\frac{q(\mathcal{M}|\mathcal{M}')}{q(\mathcal{M}'|\mathcal{M})}$$

reduces α if state \mathcal{M}' is easy to reach from \mathcal{M} and increases α if it is easy to get back to \mathcal{M} from \mathcal{M}' , thus compensating the fact that some states are easier

to reach than others. The full optimization algorithm is displayed below.

Input: Start with shortest path initialized fiber set \mathcal{M}
while temperature $T >$ temperature T_{min} **do**
 Randomly select a fiber
 Randomly select a proposal
 Generate a new state \mathcal{M}'
 Compute $\alpha = \frac{P(\mathcal{M}'|D)q(\mathcal{M}|\mathcal{M}')}{P(\mathcal{M}|D)q(\mathcal{M}'|\mathcal{M})}$
 if $\alpha > 1 \parallel \alpha > u \sim U(0, 1)$ **then**
 accept new state $\mathcal{M} \leftarrow \mathcal{M}'$
 else
 reject new state
 end if
 reduce temperature
end while

Output: Final state of the model \mathcal{M}_{final}

Two different proposals were considered to generate the new states

- Movement of a fiber's control point
- Change a fiber's weight

The new state was chosen according to a Gaussian distribution $N(0, \sigma^2)$ making them symmetric, i.e, $q(M'|M) = q(M|M')$ reducing the acceptance probability in (14) to

$$\alpha = \frac{P(\mathcal{M}'|D)}{P(\mathcal{M}|D)} \quad (15)$$

The parameter σ is the Gaussian distribution could be one of three values: σ_{GM} , σ_{WM} or σ_{weight} , depending on if the chosen proposal's distribution: moving a control point in white matter, gray matter or changing a fiber's weight.

The input of the model consisted of the set of plausible connections, all with a weight of $w = 0$, which is equivalent to an empty set. So by randomly selecting an untouched fiber and changing its weight basically meant inserting a new fiber into the model. If a fiber with weight $w = 0$ was chosen to move its control point, it was instead assigned a random value for its weight in order to not waste iterations.

3.2 Model Parameter Selection

3.2.1 Proposal Parameters

It was especially important to choose the σ -parameters σ_{GM} and σ_{WM} wisely. They could not be set too high because that would result in the proposal constantly moving the control points outside of the white and gray matter, resulting in too many rejected proposals. If they were set too small then the proposals would not explore the possible solutions fast enough, resulting in much longer time to find the optimal solution.

Since the regions of interest in the brains gray matter were much smaller than in the white matter, the Gaussian determining the step size in the gray

matter was set to half the width of the one for the white matter. The third parameter σ_{weight} was initially set 1.

3.2.2 Spline and Gaussian Smoothing Parameters

These parameters were chosen by running the method over a plausible interval of each parameter and choosing the one which gave the lowest cost function of the end result. The segment length of the spline was a compromise between computational speed and accuracy. The segment length was evaluated on the interval of $l = [0.5, 2]$ because larger segments than 2 would be larger than the voxels and cause the fiber not to be a good representation. It turned out by looking at the end results in figure 19, that a segment length of $l = 2$ gave the lowest cost function.

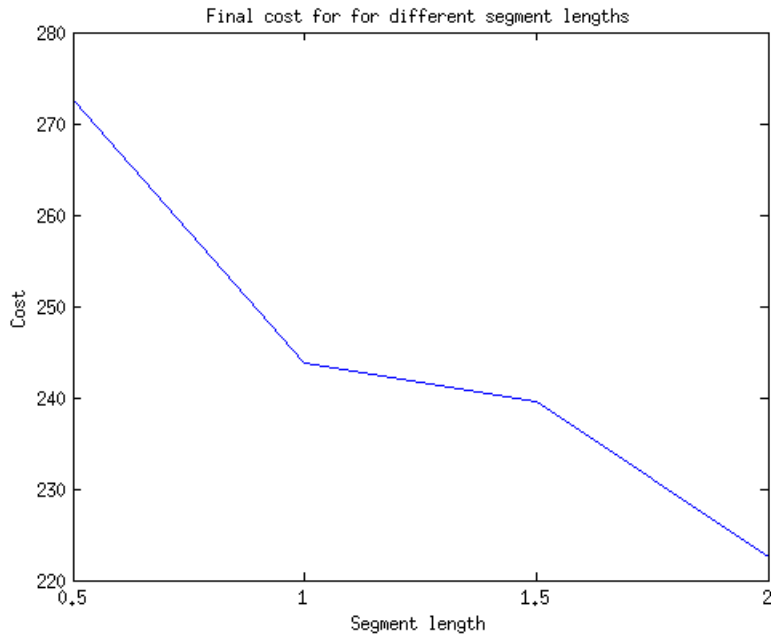


Figure 19: Plot of the different final costs for some values of segment lengths

The size of the parameter σ_{smooth} controlling the size of the Gaussian smoothing distribution was also a trade-off between speed and accuracy. If σ_{smooth} was set too high, then each fiber segment would have a much larger contribution in neighboring voxels. This leads to the method being too computationally expensive. A small value of σ_{smooth} makes each segment contribute very little, requiring a larger number of fibers to correctly reconstruct the ODFs for a voxel. That would again make the method too computationally expensive. The parameter was calibrated by evaluating the final value for values of σ_{smooth} on the interval $(0, 1]$. The results as shown figure 20 show that $\sigma_{smooth} = 0.3$ turned out to give the lowest cost function.

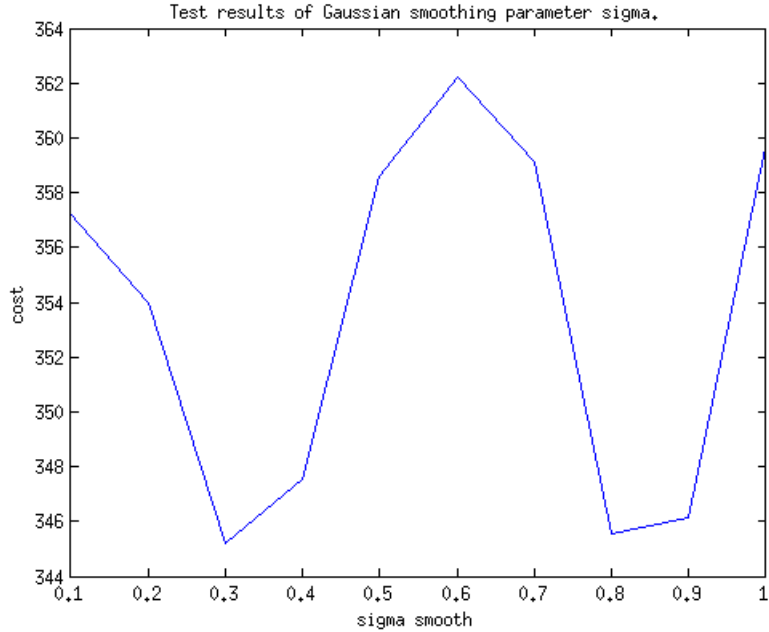


Figure 20: Calibration of Gaussian smoothing σ_{smooth} parameter. The value giving the lowest cost was $\sigma_{smooth} = 0.3$

3.3 Implementation

The algorithm was implemented in C++ with much effort put into the code running as fast as possible. A key feature was to precompute kernels for the most time consuming operations, namely: calculating the Gaussian smoothing, the temperature cooling scheme of the simulated annealing procedure and calculation of each voxels ODF. A consequence of this was that the reconstructions were more sparse because the computed input vales for each kernel was rounded to the nearest pre-calculated value.

3.4 Datasets and Evaluation

The method was tested on two datasets: one phantom dataset called the FiberCup and one in-vivo data set of a human brain. Since it is currently not possible to know the ground truth of the in-vivo dataset, global tractography methods are currently scored on the FiberCup data set after a method called the Tractometer [5] which will be explained later in this section. The test on in-vivo data was primarily to evaluate its speed and make sure that the method actually generates a connectome to study and generate some network parameters to study.

3.4.1 FiberCup

The FiberCup is a phantom designed for a tractography contest at the MICCAI conference held in London in 2009 [26]. It is now an open and widely used dataset to test tractography methods on. The phantom itself consisted of 12 regions of interest and seven connections containing many of the problematic fiber scenarios such as crossing, kissing and blending of fiber configurations. The phantom was acquired in 64 directions at $b = 1500s/mm^2$ and $3 \times 3 \times 3$

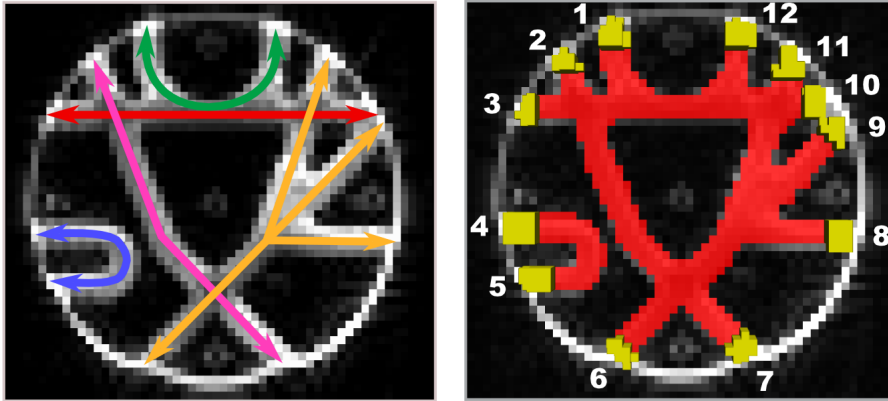


Figure 21: The FiberCup data. The left image shows the ground truth of the seven connections. The right image shows the tracking mask used with the regions of interest. The red color represents the white matter, the yellow color represents the gray matter [7].

mm in plane resolution, acquiring three 3 mm slices.

3.4.2 Tractometer

The tractometer is a methodology proposed in [5], which is an evaluation system for tractography with a particular emphasis on global connectivity. It involves counting and keeping track of:

- *True Connections (TC)*: fibers connecting expected ROIs. TC will be reported in percentage of true connections.
- *False but Plausible Connections (FPC)*: fibers connecting unexpected ROIs not corresponding to the ground truth. It is also reported in percentage. These connections are especially important to score as they look anatomically good but are in fact incorrect.
- *Wrong connections (WC)*: fibers that are incomplete and don't connect two ROIs. We expect this count to be zero for our method due to the anatomical priors.
- *True Bundles (TB)*: a bundle is the collection of fibers connecting two ROIs. This score counts the total number of correct connected ROIs.
- *Wrong but plausible bundles (WPB)*: counts the number of bundles connecting two ROIs which are not supposed to be connected.

3.4.3 In-vivo Brain Data

The in-vivo diffusion measurements were acquired on a Siemens 3T Trio. The whole brain was covered with 51 contiguous 2 mm slices with an in-plane resolution of $2 \times 2 \times 2$ mm. The diffusion measurements were performed in 64 directions with an effective b-value of $b = 3000 \text{ s/mm}^2$. Segmentation of the gray matter (GM) and white matter (WM) mask was done using from the T_1 data set using established methods. The gray matter was divided up into 83 regions based on anatomical functions [8] using the well known neuroimaging software package known as *freesurfer* (surfer.nmr.mgh.harvard.edu).

4 Results and Discussion

Once the method was implemented and parameters fine tuned to the above values, it was run ten times on the FiberCup dataset and one time on the in-vivo brain data.

4.1 FiberCup Dataset

In the latest competition which evaluates global tractography methods on the FiberCup [14], the Gibbs tracker was the best performing model, making its suitable benchmark for the method derived in this thesis.

The proposed method took around 15 minutes to run on a conventional laptop using an Intel[®] Core[™]i7-2630QM CPU @ 2.0 GHz. Compared to the Gibbs tracker which takes about 40 minutes to run, this is a considerable improvement much thanks to the reduced computational burden using the spline formulation.

The evolution of the cost for all ten runs is shown in figure 22 while the mean all ten runs is shown in figure 23. We see that the method converges after about $3 \cdot 10^6$ iterations.

The reconstruction of the connections in the FiberCup shown in figure 24 where the individual connections have been isolated.

Recall that each fiber has a weight which cannot be shown by figure 24. The weighted connection matrices in figure 25 complements figure 24 by summing the weights of all the fibers in each connection.

The reconstruction successfully reconstructs all the true connections (which

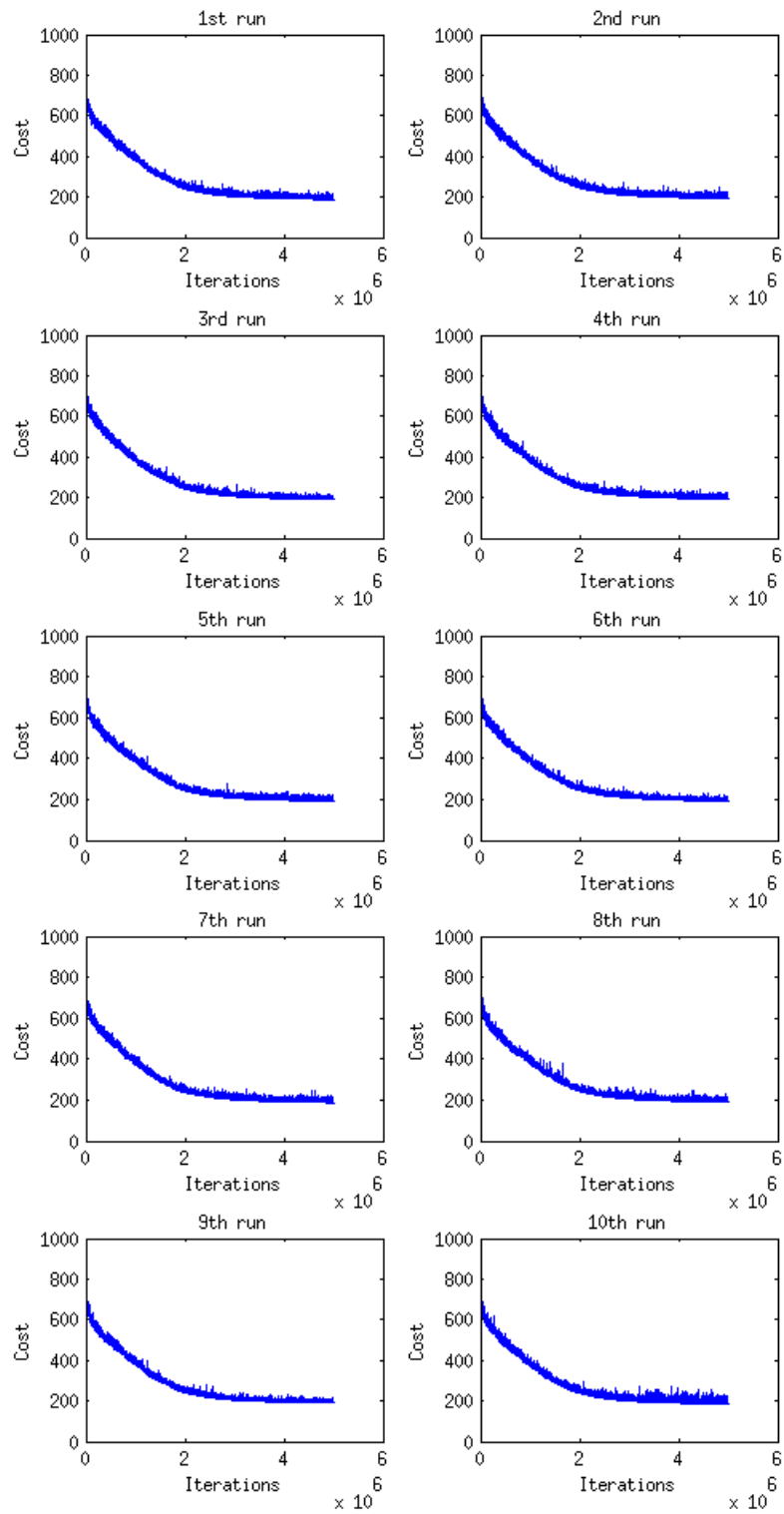


Figure 22: Figure showing the evolution of the cost function for all ten iterations of the method

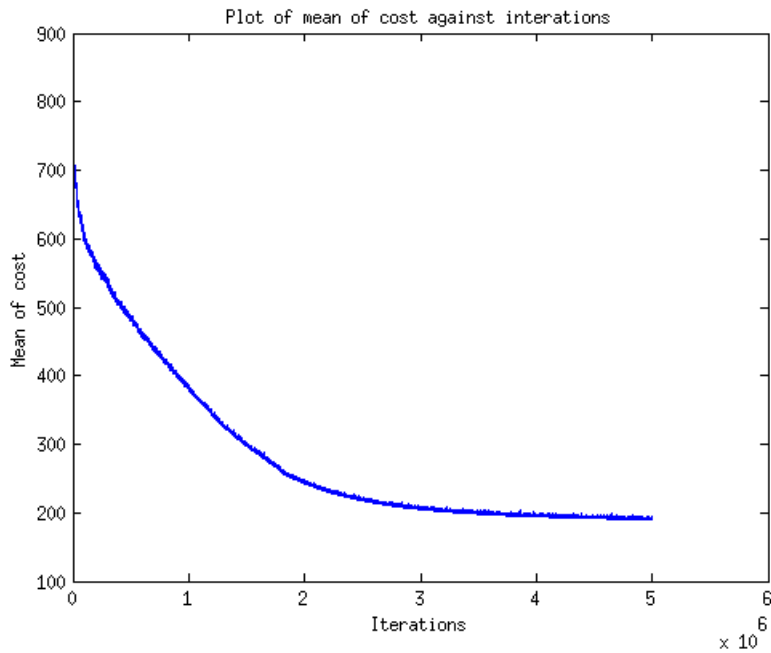


Figure 23: Figure showing the mean of the evolution of the cost function for all ten iterations of the method

can be identified in figure 21) but struggles with the "kissing" connections [1 – 12], [3 – 10], [1 – 10], [3 – 12]. Here we expect [1 – 12], [3 – 10] to be stronger than [1 – 10], [3 – 12]. The major reason for this result is that for all of the fibers in these connections, the majority of the segments still fits the data in each voxel relatively well and it is only in occasional voxels where the model fits the signal poorly. Therefore the method struggles to distinguish between a correct and an incorrect fiber as both will give a relatively similar low cost. This is one of the major improvement areas for the method in it's current state. The method does still however produce less incorrect fibers than the Gibbs tracker who's reconstruction of the 14 most prominent bundles are shown below in figure 26 which is a noticeable improvement.

The coefficient of variation defined as the ratio of the standard deviation σ to

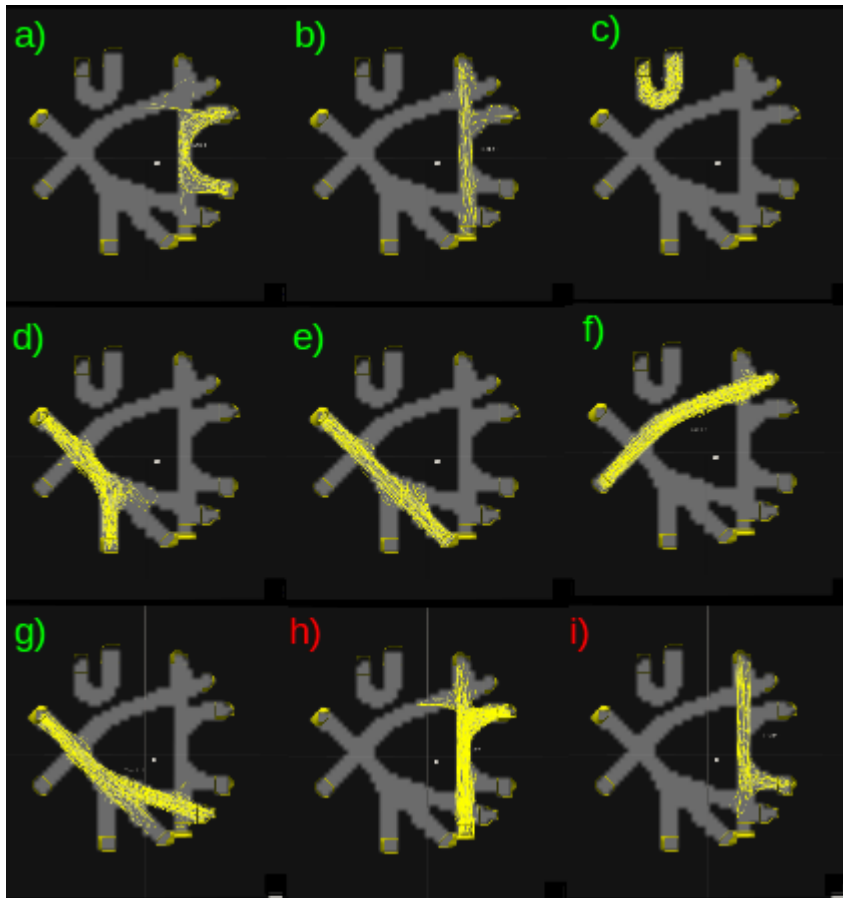


Figure 24: The figure shows the reconstruction of all the fiber bundles reconstructed by the method. Figure a-g shows the correct connections and h-i shows false but plausible connections.

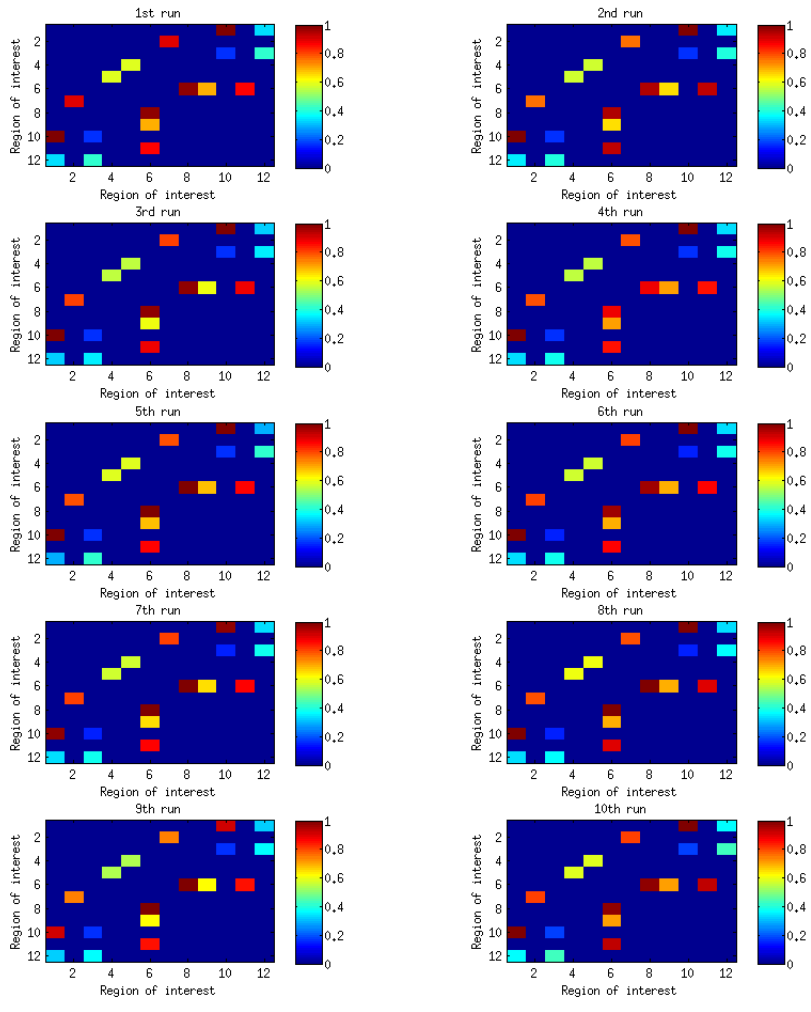


Figure 25: Weighted connection matrices showing the strength of the connection between two ROIs as the sum of the weights of all the fibers connecting them. The weights have been normalized against the strongest connection which has the value 1.

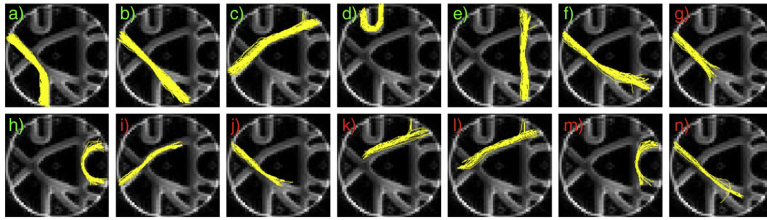


Figure 26: The figure shows the reconstruction of all the fiber bundles reconstructed by the Gibbs tracker. It is clear that the Gibbs tracker reconstructs more incorrect fiber bundles [7].

the mean μ :

$$c_v = \frac{\sigma}{\mu} \quad (16)$$

can be used to measure the extent of the variability of each connection determining how the results vary in each run. Figure 27 compares the coefficient of variation of our method with the Gibbs tracker in each connection. Clearly, our developed method has a lower variability between the runs and is thus more stable than the Gibbs tracker by converging to the same answer more often.

Next we evaluate our method according to the tractometer. Table 1 compares our method’s reconstruction to the Gibbs tracker, where the results of the Gibbs tracker were taken from [7].

	<i>Gibbs</i>	<i>Our method</i>
TB	7	7
FPB	12.5	2.8
WC (%)	76.5	0
TC (%)	19.8	75
FPC (%)	3.7	25

Table 1: Tractometer scores for our method compared to the Gibbs tracker.

As we can see, the introduction of anatomical priors completely removes all of the wrong connections while having a high percentage of true connections and identifying a fewer number false but plausible bundles of Gibbs. However normalizing the Gibbs fibers by the number of actual connecting fibers (1-WC), the number of true connections (TC) for Gibbs is actually 84.3% and 15.7% false but plausible connections (FPB), which although initially seems better than our method is not fair comparison; as our method has weights on the reconstructed fibers, while the Gibbs tracker’s fibers do not. A better comparison would be instead of a binary threshold to only include fibers reconstructed with our method which have a high enough weight. Further research must be done first to identify what this threshold should be.

In the end, even if the Gibbs tracker does produce a higher number of true connections, the fact that it also produces a high number of false but plausible

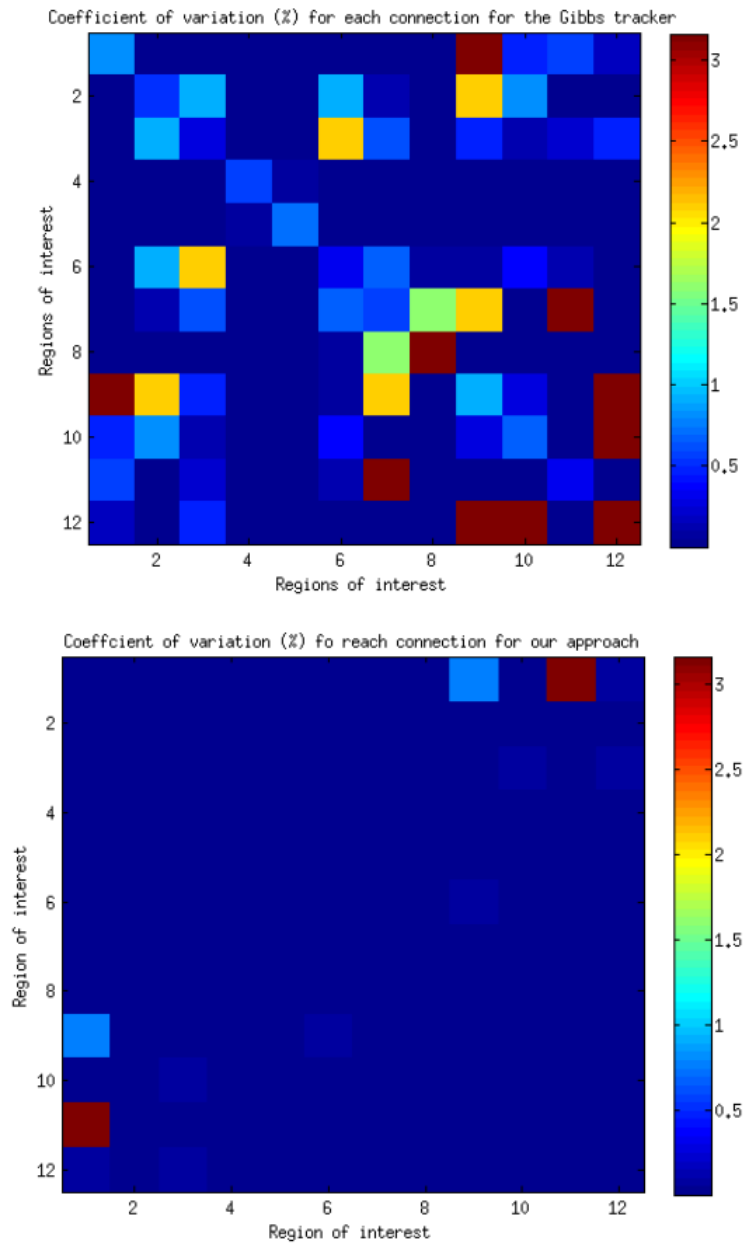


Figure 27: The figure shows the coefficient of variation for each connection for ten runs. Top: The Gibbs tracker. Bottom: Our method.

connections makes the Gibbs tracker method more difficult to use for connectome analysis compared to our method.

4.2 In-vivo Data

For the in-vivo dataset the iterations had to be raised by a magnitude of 10 to 10^7 iterations due to the sheer size of the dataset. The simulation took approximately 2 hours which is half of the time that Gibbs tracker which takes 4 hours. Figure 28 shows the front, side and top view of the entire reconstruction along with certain bundles segmented out.

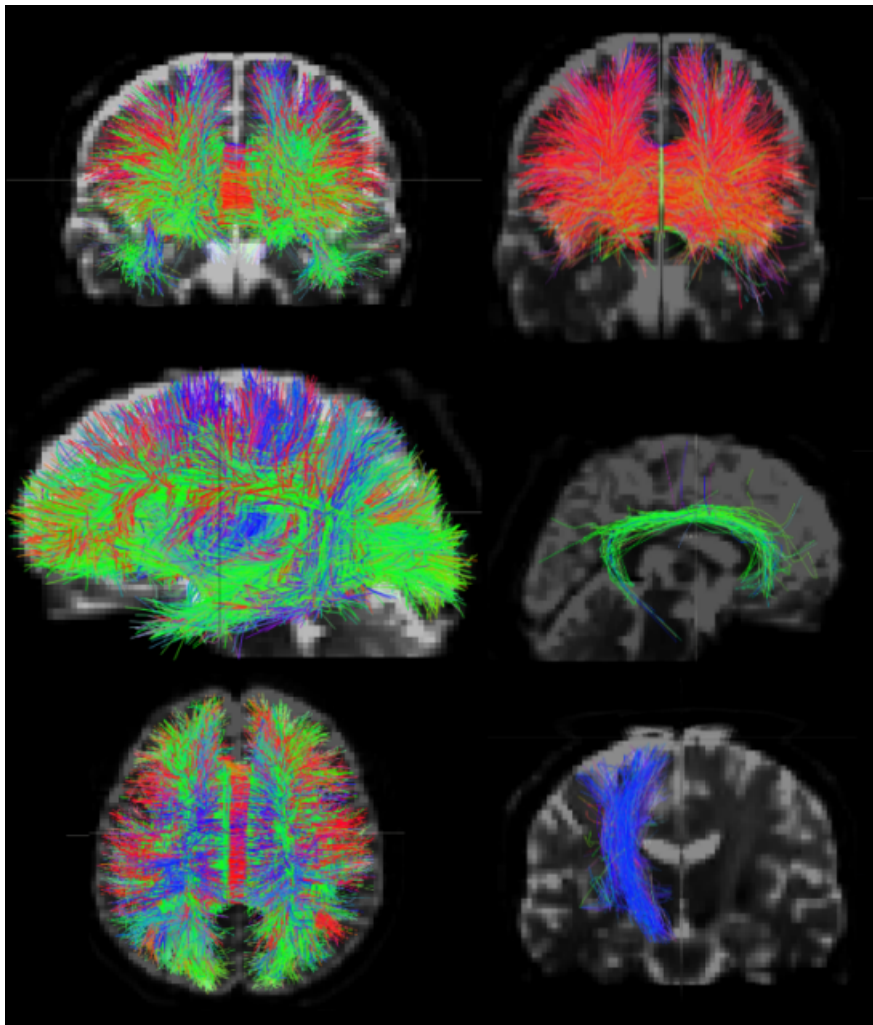


Figure 28: The left column shows the entire reconstruction of all the Fiber bundles. The right column shows the reconstruction of the Fiber bundles through the Corpus Callosum (top red), the cingulate cortex (middle green) and the Corticospinal tract (bottom blue).

The weighted connection matrix was derived from the weights of the reconstructed fibers and is displayed in figure 29

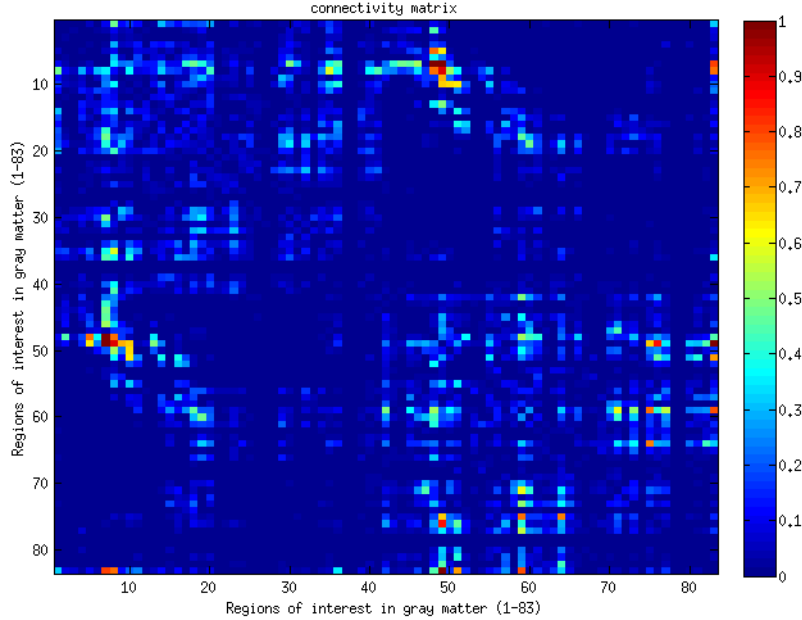


Figure 29: The weighted connection matrix displaying the connection strength between the 83 regions of interest. The connection strengths has been normalized against the strongest connection, giving it the value 1.

From the connection matrix the network parameters used to evaluate the network can be derived. In this dataset with 83 regions of interest, it will be difficult to view the local values for each individual node and we will focus on the global values. Usually these 83 regions of interest are grouped into clusters corresponding to what regions are to be studied. But since this thesis has focused on global reconstruction the dataset contained the 83 regions unclustered.

Global Network Parameter	value
Mean strength (k)	3.3973
Clustering coefficient (C)	0.0416
Characteristic path length (L)	0.0128

Table 2: Global network parameters derived from the connectivity matrix.

Further analysis of these network parameters is beyond the scope of this thesis, but procedure is normally to compare the local and global network parameters to healthy and pathological brain s in order to determine the condition of the brain connectivity.

5 Conclusions

In this thesis we have developed a new global tractography algorithm which performs better than the state of the art method, the Gibbs tracker in the tests used to score these kinds of methods. However, the method still has problems not removing enough wrong but plausible connections and needs additional improvements and refinements in order to do this. Unfortunately, simply increasing the number of iterations is not an obvious remedy as the solution space of the problem is so large that there is no guarantee of convergence within a feasible amount of time. The two obvious ways of going forward are: decreasing the solution space and more efficient exploration of the distribution. To do this two main improvements are proposed:

- Start with a better solution
- Improve proposals

Initial Solution

Currently the method starts with all the initialized fiber weights set to zero. This creates an enormous space to explore, especially for real brain data where the plausible fibers are about $5 \cdot 10^5$. The possibility should be explored to start the sampler with a set of plausible prior weights just as for the anatomical priors for the connections. This will greatly decrease the number of incorrect states that the Markov Chain has to traverse through before reaching the region around the optimal solution. It has been proven possible to optimize the weights given a stationary setup using convex optimization [7]. This information should perhaps be incorporated into the prior.

Proposal Improvements

There are ways to more efficiently generate correct candidates thus increasing convergence speed using Hybrid Monte Carlo methods [21]. These are methods where the proposals can be skewed to propose candidates with a higher acceptance rate thus resulting in a more efficient exploration of the distribution and faster convergence.

With these improvements we will hopefully have a state of the art method which not only can be used for better reconstructions of fiber tracts but also a method capable of studying the evolution of the connectome by exploring the state of the connectome around an optimal solution in order to study how the brain network parameters are affected. This has never previously been done but would be of great interest to the diffusion MRI community.

References

- [1] Alba C. *Statistical Analysis for Global Tractography*. EPFL, 2013.
- [2] Le Bihan D., Mangin JF., Poupon C., and al. *Diffusion Tensor Imaging Concepts and Applications*. Journal of Magnetic Resonance Imaging, 2001.
- [3] Bihan D. *Looking into the Functional Architecture of the Brain with Diffusion MRI*. Nature reviews Neuroscience, 2003.
- [4] Ciccarelli O., Catani M., Johansen-Berg H., Clark C., and Thompson A. *Diffusion-based Tractography in Neurological Disorders: Concepts, Applications, and Future Developments*. ScienceDirect, 2008.
- [5] Côte M-A, Borè A., Girard G., Houde J-C., Descoteaux M. *Tractometer: On-line Evaluation System for Tractography*. Université de Sherbrooke, 2012.
- [6] Twigg, C *Catmull-Rom Splines* Carnegie Mellon University 2003.
- [7] Daducci A., Dal Palu A., Lemkaddem A., Thiran J-P. *A Convex Optimization Framework for Global Tractography*. Biomedical Imaging, 2013.
- [8] Daducci A., Gerard S., Griffa A., Lemkaddem A., Cammoun K., Gigandet X., Meli R., Hagmann P., Thirion J-P. *The Connectome Mapper: An open Source Processing Pipeline for Connectomes with MRI*. PLoS ONE, 2012.
- [9] Dijkstra E.W. *A Note On Two Problems in Connexion with Graphs*. Numerische Mathematik, 1959.
- [10] Douglas D., Peucker T. *Algorithms for the Reduction of the Number of Points Required to Represent a Digitized Line or its Caricature*. The Canadian Cartographer, 1973.
- [11] Einstein A. *Investigations on the Theory of the Brownian Movement*. New York, NY: Dover 1956.
- [12] Ferrerira-Santos F. *Complex Network Analysis of Brain Connectivity: An introduction*. University of Porto, 2012.
- [13] Fillard, P., Poupon, C., Mangin, J.F. *A Novel Global Tractography Algorithm Based on an Adaptive Spin Glass Model*. Medical image computing and computer-assisted intervention, 2009.
- [14] Fillard, P., Descoteaux, M., Goh, A., Gouttard, S., Jeurissen, B., Malcolm, J., Ramirez Manzanares, A., Reisert, M., Sakaie, K., Tensaouti, F., Yo, T., Mangin, J.F., Poupon, C. *Quantitative Evaluation of 10 Tractography Algorithms on a Realistic Diffusion MR Phantom*. Neuroimage, 2011.
- [15] Hagmann Patric. *From diffusion MRI to Brain Connectomatics*. EPFL, 2005.
- [16] Hagmann P., Jonasson L., Maeder P., Thiran J-P., Wedeen V.J., and Meuli R. *Understanding Diffusion Mr Imaging Techniques: From Scalar Diffusion-Weighted Imaging to Diffusion Tensor Imaging and Beyond*. RadioGraphics, 2006.

- [17] Jbabdi S., Woolrich MW., Andersson JL., and Behrens TE. *A bayesian framework for global tractography*, *Neuroimage*, 2007.
- [18] Kreher B.W., Mader I., Kiselev V.G. *Gibbs Tracking: A novel Approach for the Reconstruction of Neuronal Pathways*. *Magnetic Resonance in Medicine*, 2008.
- [19] Björnemo M., Brun A. *White Matter Fiber Tracking Using Diffusion Tensor MRI*. Linköping University 2002
- [20] Longchuan L., Rilling J., Preuss T., Glasser M., Damen F., Xiaoping H. *Quantitative Assessment of a Framework for Creating Anatomical Brain Networks via Global Tractography*. *Neuroimage*, 2011.
- [21] Makay D. *Information Theory, Inference and Learning Algorithms*. Cambridge, 2003.
- [22] Mori S. and Van Zijl P. *Fiber Tracking: Principles and Strategies - a Technical Review*. Wiley InterScience, 2002
- [23] Mori S., Crain B., Chacko V., and Zijl PV. *Three-Dimensional Tracking of Axonal Projections in the Brain by Magnetic Resonance Imaging*. *Annals of Neurology*, 1999.
- [24] Neal R.M. *Probabilistic Inference Using Markov Chain Monte Carlo Methods*. University of Toronto, 1993.
- [25] Parker G.J., Haroon HA., and Wheeler-Kingshott CA. *A Framework for a Streamline Based Probabilistic Index of Connectivity Using a Structural Interpretation of MRI Diffusion Measurements*. *Neuroimage* 2003.
- [26] Poipon C., Rieul B., Kezele I., Perrin M., Poupon F., Mangin J-F. *New Diffusion Phantoms Dedicated to the Study and Validation of High-Angular-Resolution Diffusion Imaging (HARDI) Models*. *Magnetic Resonance Imaging in Medicine*, 2008.
- [27] Reisert M., Mader I., Anastasopoulos C. *Global Fiber Reconstruction Becomes Practical*, *Neuroimage* , 2011.
- [28] Tuch D., Reese T., Wiegell M., Makris N., Belliveau J., Wedeen J. *High Angular Resolution Diffusion Imaging Reveals White Matter Fiber Heterogeneity*. *Magnetic Resonance in Medicine* 2002.
- [29] Sköld Martin. *Computer Intensive Statistical Methods*. Lund University, 2006.
- [30] Sporns O. *Networks of the Brain: Quantitative Analysis and Modeling*. Indiana University, 2010.

Master's Theses in Mathematical Sciences 2014:E6
ISSN 1404-6342

LUTFMS-3238-2014

Mathematical Statistics
Centre for Mathematical Sciences
Lund University
Box 118, SE-221 00 Lund, Sweden

<http://www.maths.lth.se/>